Politecnico di Torino

Master Thesis

A Mean-Field Games Application to Pedestrian Dynamics

Author:
Matteo Butano

Supervisor:
Prof. Denis Ullmo

Master of Science
Physics of Complex Systems

October 12, 2021

ABSTRACT

This thesis will focus on the topic of pedestrian dynamics. It will start presenting the experiment that inspired this research, performed in France and Argentina, that consisted in the analysis of the crowd's response to the passage of a cylindrical intruder in a controlled environment. The way this experiment contradicted expectations motivated the research of a theoretical explanation of what was observed. The research group I belong to tried to use Mean-Field Games (MFG) to explain the experiment. The second part of this thesis will therefore present the basis of MFG and its main features, with the description of the mathematical foundations and the physical interpretation of the results. Finally, the third part of this thesis reports the results we obtained in our attempt to model the experiment with Mean-Field Games. We will first explain the approach we chose to follow and then we will report the analytical solution and comment of the results. Given the simplicity of the model we used we are pretty happy with the results we obtained. There is still plenty to improve, but this is another story that will hopefully be told in the future.

RINGRAZIAMENTI

Ringrazio tutti coloro che ho conosciuto in questi anni e che mi hanno insegnato molto, tutti coloro che già conoscevo e che hanno continuato a rimanermi accanto, tutti coloro che non ci sono più.

Forse un mattino andando in un'aria di vetro,
arida, rivolgendomi, vedrò compirsi il miracolo:
il nulla alle mie spalle, il vuoto dietro
di me, con un terrore di ubriaco.

Poi come s'uno schermo, s'accamperanno di gitto
alberi case colli per l'inganno consueto.
Ma sarà troppo tardi; ed io me n'andrò zitto
tra gli uomini che non si voltano, col mio segreto.

- Eugenio Montale

Contents

1 Introduction **1**
- 1.1 The Experiment . . . 2
- 1.2 Model Comparison . . . 4

2 Mean-Field Games **7**
- 2.1 The main equations . . . 7
- 2.2 Changes of variables . . . 10
- 2.3 Operator formalism . . . 12
- 2.4 Exact results . . . 14
  - 2.4.1 Non interacting case . . . 14
  - 2.4.2 Local attractive interaction . . . 15
  - 2.4.3 Quadratic external potential . . . 16

3 MFG model of the experiment **19**
- 3.1 Passing to the moving frame . . . 19
- 3.2 Choosing boundary condition . . . 21
- 3.3 Numerical solution . . . 22
- 3.4 Results . . . 23

4 Conclusions **27**
- 4.1 Reproducing the experiment . . . 27
- 4.2 Simulating other scenarios . . . 29
- 4.3 Final remarks and future improvements . . . 31

List of Figures

1.1 Snapshot of one of the performed experiments. The left figure shows the detection of participants using colored hats in Orsay, France. The right figure shows the numerical representation of the data. Images from [1] 2

1.2 The density of pedestrians is displayed for three different average densities and in the two experimental set-ups: when people face the intruder they react more quickly than when they are oriented randomly, making space for the intruder and then closing behind him. Images from [1]. 3

1.3 The figure shows the velocity field of pedestrians facing the intruder in case of sparse (left column, $\bar{\rho} \sim 1.5\,\mathrm{ped}/m^2$) and dense (right column, $\bar{\rho} \sim 6\,\mathrm{ped}/m^2$) environments. Images from [1]. 4

1.4 The picture shows the density and the velocity plot obtained with granular matter algorithm. On the left we have a short-time anticipation based algorithm, which gives particles some predictive ability. On the right we have instead the results of pure granular matter with no anticipation ability. 6

3.1 The relations between healing length, healing speed and the velocity and size of the obstacle identify four different regimes. 25

3.2 The relations between healing length, healing speed and the velocity and size of the obstacle identify four different regimes, velocity plots. 26

4.1 Here are displayed both the density and the velocity field of the pedestrians. Our goal was to obtain a visually similar result to figure 1.2-b 28

Chapter 1

Introduction

We all have experience with crowded environments. Although we did not always realize it, many of these spaces are designed on purpose to make us follow certain trajectories. Public spaces designers, in fact, have been using simulations to predict the flow of pedestrians for a long time. These predictions are then used to place wisely obstacles and doors, decide the length of corridors etc. in order to enhance safety. The underlying algorithms, however, are built to simulate human behavior using techniques of granular matter [16], [32], or fluid dynamics [30]. These approaches ultimately give reasonable results, but only for macroscopic quantities such as escape time, or to have a visual impression of the phenomenon. However, there are cases in which such models fail. In this thesis I will present a new and promising approach to the problem of pedestrian dynamics. So far, little attention was paid to the *psychology* of individuals, in the sense that the property of humans is to have a higher abstract intelligence than any other living species. This is what makes us able to use the little information we have about the present to build one or multiple future scenarios in order to better allocate resources. More concisely, humans can develop strategies, anticipating what is going to happen and deciding how they will behave in advance. This feature of humans' intelligence was captured for the first time by the works of John Nash, when he introduced in a mathematically rigorous way the concepts of game theory. At the hearth of this approach lies indeed the notion of Nash equilibrium, a more informed and evolved way to intend the *best* strategy. What is fundamental is in fact to make clear what is best, and in which sense. Game theory allows to quantify a best which is not *absolute*, but *relative to others*. This turns out to be a more stable solution to the problem of optimization, and example of this are found everywhere in Nature. We thought to extend the field of its applications and include in the list the problem of predicting and simulating pedestrian dynamics.

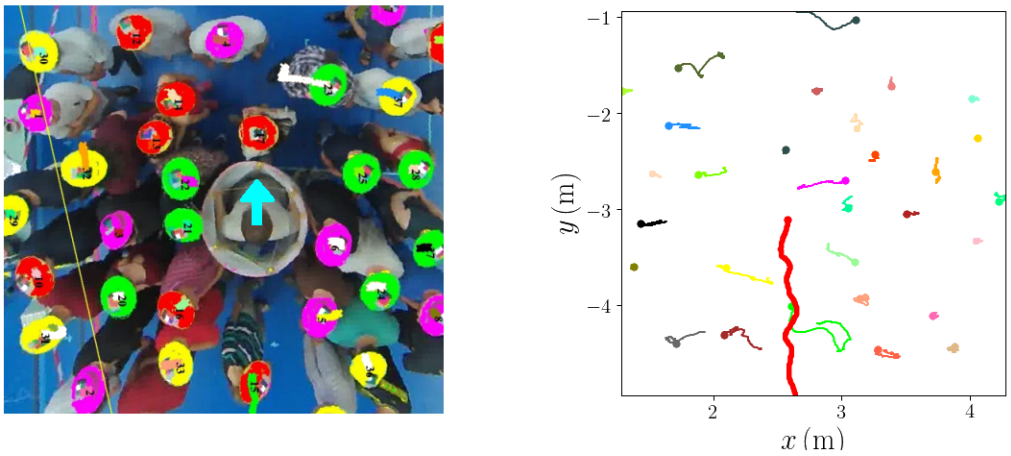

Figure 1.1: Snapshot of one of the performed experiments. The left figure shows the detection of participants using colored hats in Orsay, France. The right figure shows the numerical representation of the data. Images from [1]

1.1 The Experiment

In 2019 the work of Nicolas et al. [1] reported a simple but very pedagogical example in which the usual pedestrian dynamics softwares would fail to predict the correct behavior of the crowd. Two experiments, performed in 2017 in Orsay (France) and Bariloche (Argentina) and involving between 35 and 40 participants of various ages, consisted in the analysis of the crowd's response to the presence of a single moving cylindrical obstacle. The crowd stood in a delimited square area with side of approximately 4 meters and, with different pedestrian densities, the obstacle was made pass through. Figure 1.1 shows how the experiments were actually performed. One participant wore a cylinder, of diameter 74cm in France and 68 cm in Argentina, and walked his way through the crowd. Moreover, the people in the crowd were asked to arrange in two configurations: in one case they were asked to face the intruder, in the other to stay in randomly oriented positions. In the work of Hoogendoorn and Bovy [33] the decision process of pedestrians moving in full-scale public environments is divided into three different levels. The first is the *strategic* level, which corresponds to the choice of where inside the area pedestrians will head to; the choice of the route to follow to reach the decided place attains to *tactical* level; finally, how to move along the chosen route, to avoid obstacles for example, is what is called the *operational* level. The experiment that I am presenting here clearly does not aim at reproducing a full-scale public space, whereas it focuses on what could be one of its elements; it therefore studies the *operational* decision level of pedestrians. As we can see in figure 1.2, the intruder caused a depletion in density both in front and behind it, and an increase at its

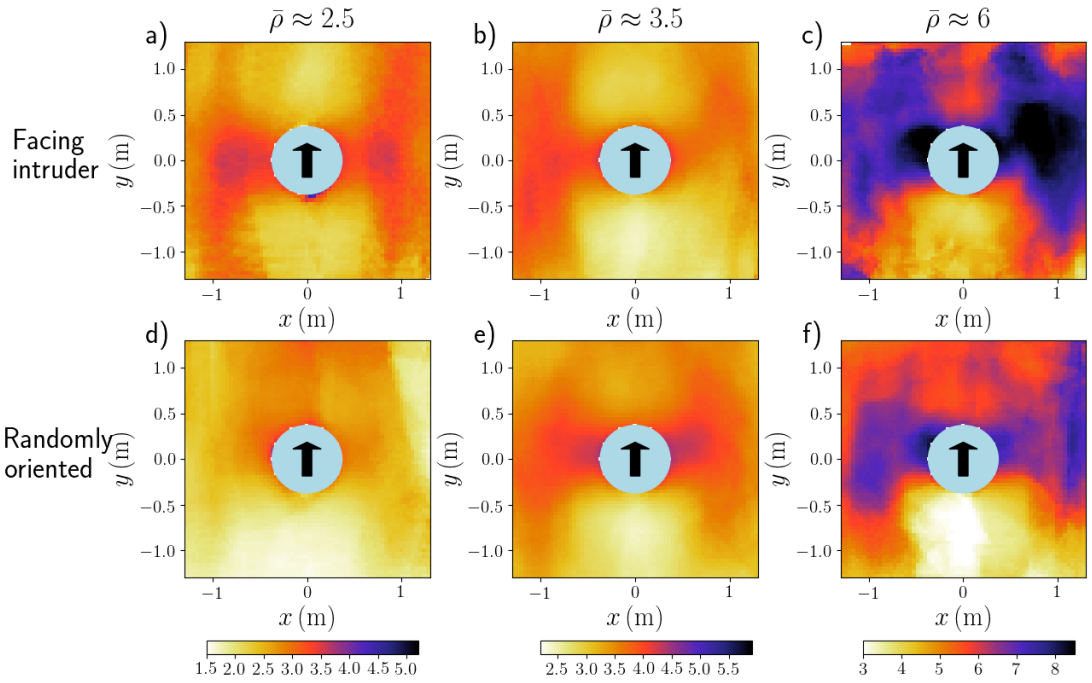

Figure 1.2: The density of pedestrians is displayed for three different average densities and in the two experimental set-ups: when people face the intruder they react more quickly than when they are oriented randomly, making space for the intruder and then closing behind him. Images from [1].

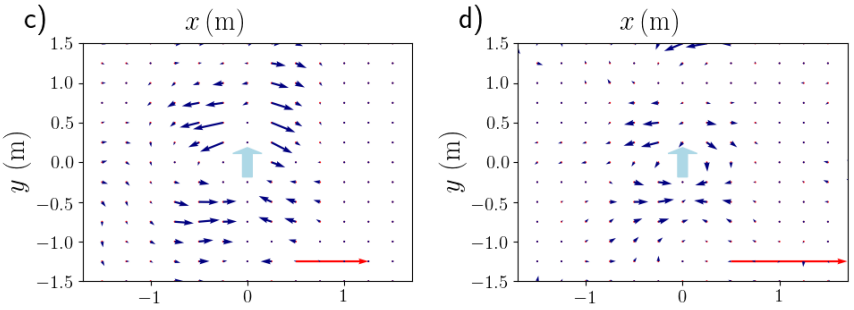

Figure 1.3: The figure shows the velocity field of pedestrians facing the intruder in case of sparse (left column, $\bar{\rho} \sim 1.5\,\mathrm{ped}/m^2$) and dense (right column, $\bar{\rho} \sim 6\,\mathrm{ped}/m^2$) environments. Images from [1].

sides. This means that people actively avoided hitting the cylinder by leaving it room to pass, but tried not to go too far from their original position to stay away from the crowed surrounding as well. This is very well confirmed by what is shown in figure 1.3, where it is clearly displayed that people moved laterally to avoid impact. Moreover, people started to move quite far away from it, as the picture on the left of figure 1.3 shows. This is fundamental in our analysis, in that it shows that pedestrians (humans or highly efficient information processors) decided to accept to be uncomfortable for a limited period, since moving perpendicularly to the obstacle meant pushing against the surrounding crowd, in order to avoid impact with the intruder as completely as possible. Moreover, this shows also the long term anticipation ability of pedestrians. In fact, by predicting the complete path of the obstacle, they knew that any motion with a component parallel to the direction of the intruder would have been useless in avoiding it. These elements of what we could call the psychology of humans are very distinctive of our ability to see in the future. In the end, for those standing in the direction of the cylinder, the fact that they *knew*, or *predicted*, even when it was still far away, that the obstacle would have eventually approached them, is what ultimately convinced them that moving laterally towards the crowd was the *optimal* choice.

1.2 Model Comparison

The main goal of this research project is to propose a new and efficient method to reproduce the experimental discoveries that I just introduced. However, one may argue that there already exists efficient ways to simulate pedestrian dynamics, so why should one care. Fortunately, thanks to Antoine Seguin and Iñaki Echeverría Huarte who produced the simulations I will now discuss, it is clear that conventional pedestrian dynamics software would fail at such a task. In fact, pedestrians

have often been studied as particles in a constrained environment and therefore in first approximation simulated as such. Although this could give good insights into macroscopic behavior, such as escape time, in large and not complex environments, simple granular matter simulations would fail to reproduce what the experiments showed. In fact, as the right column of figure 1.4 shows, the passage of the intruder through granular matter would just push particles along its direction of motion, leaving a empty space behind and two trails of escaped particles at its sides. The velocity plot shows that all particles would move in the direction of the intruder, pushed by their neighbors and thus by the current that is generated by the passage of the intruder. What the granular approach shows is clearly not catching what the experiment portrays, both in the distribution of the density and the velocity of agents. The software usually employed by companies in the pedestrian simulation businesses, however, are not simple granular matter simulations. During the last decades many have engineered ways to get better qualitative and quantitative agreement. For example Helbing and Molnar [17] proposed a social-force model in which actual contact forces are combined with pseudo-forces (social-forces). These social-forces were originally function only of the current position of pedestrian, but this approach was then extended to make them depend also on the near future positions [18] of others. This makes agents avoid most imminent collisions through an optimization process in the velocity space. All these models are agent-based collision-avoidance algorithms that only take into account the immediate future, and, as the left column of figure 1.4 shows, this is not enough to reproduce the experiment. The density plot obtained with the short-time anticipation algorithm simulation shows the appearance of two darker areas a the sides of the obstacle, but still there is no clear depletion in front of it. Moreover, the velocity plot of the short-time anticipation simulation makes it clear that something is missing. As shown in the left-bottom picture of figure 1.4, the arrows, especially in front of the cylinder, point in its direction of motion instead of laterally, a key feature that this category of models fail to reproduce. These are the premises that convinced us of the fact that there is still plenty of room for improvement, and the next chapter will introduce how we tried to achieve it.

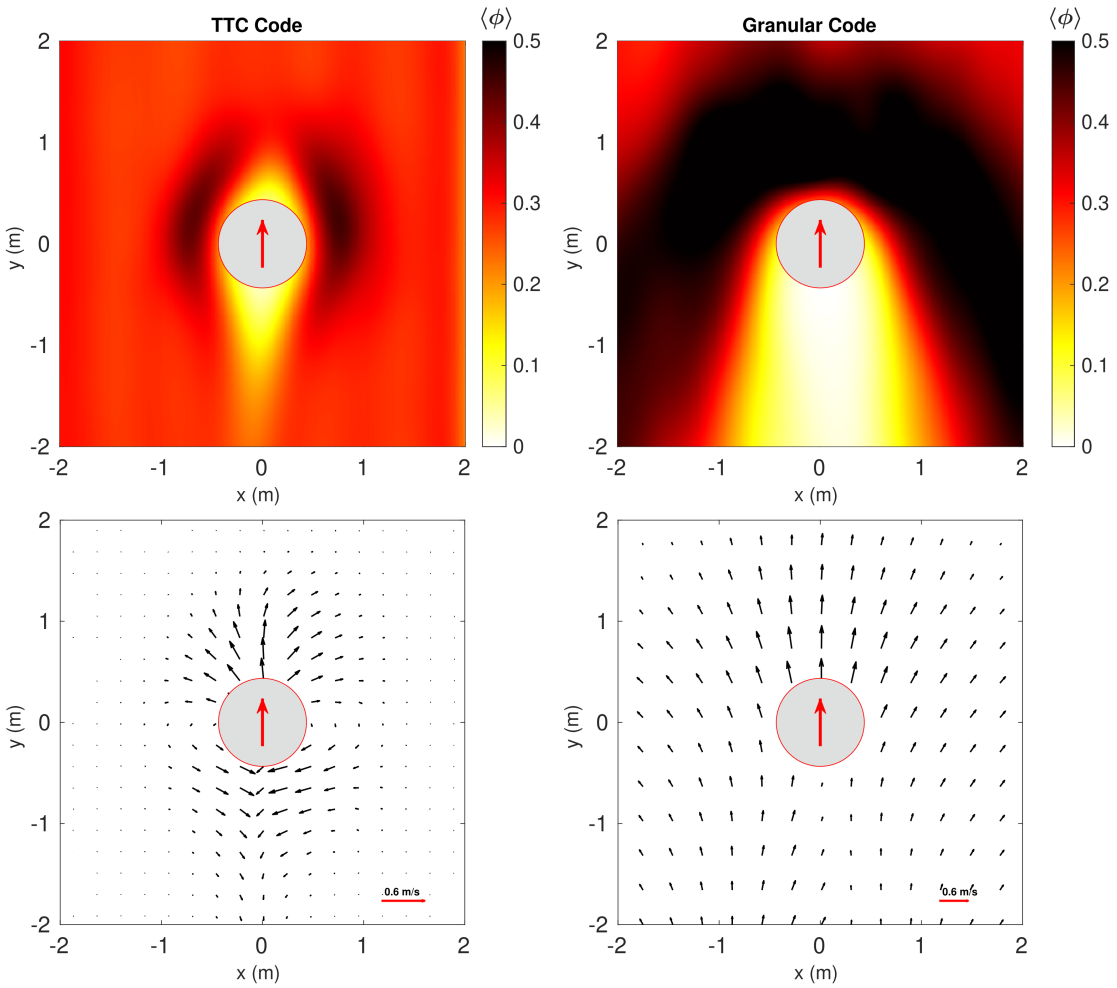

Figure 1.4: The picture shows the density and the velocity plot obtained with granular matter algorithm. On the left we have a short-time anticipation based algorithm, which gives particles some predictive ability. On the right we have instead the results of pure granular matter with no anticipation ability.

Chapter 2

Mean-Field Games

Mean-Field Games (MFG) constitutes a relatively new field of research. Its foundations are in the works of J.-M. Lasry and P.-L. Lions [27], [28], [29] and of M. Huang, R. P. Malhamé and P. E. Caines [22]. During the years, many works have been focused on for existence and uniqueness of solutions [10], [20] and the comparison between discrete games in the limit of large number of players and their mean-field analogous [8], [13], [14]. At the same time, however, improvements were made towards the elaboration of numerical schemes [3], [6], [21], to solve MFG problems. Applications of MFG are found in various areas, such as finance [11], [15], economics [2], [4], social problems like pedestrian dynamics and segregation [5], [26], and also engineering [23], [24]. This list of results suggest how this topic has attracted the attention of many researches, as it did with mine when I chose what to focus my thesis on. My work on the topic is based on the approach that D. Ullmo et al. explained clearly in [34] a couple of years ago. In this paper Ullmo and colleagues carefully explain how MFG can be linked to Quantum Mechanics (QM), in particular to the study of the Non-Linear Schrödinger Equation (NLSE), a very well established topic in Physics. The connection between the two fields, MFG and QM, is already quite interesting in itself, but what really struck me was that this approach does indeed work quite well, also considering that the nature of the phenomena explained is quite different!

2.1 The main equations

Mean-Field Games are optimally driven diffusive processes of a large number of agents. More explicitly, we consider a *differential game* that is played by a large number of *agents* N and that evolves in time. At each time t, we can associate to each agent its *state variable* $\vec{X}_i(t) \in \mathbb{R}^d$. Then, throughout the game, that starts at $t = 0$ and ends at $t = T$, every player has the possibility to change the

control parameter $\vec{a}_i(t) \in \mathbb{R}^d$, that corresponds to the choice of a strategy. We then suppose that the evolution of a player's state variable is subjected to some noise and can therefore be described using using the *Langevin equation*

$$\dot{\vec{X}}_i = \vec{a}_i(t) + \sigma_i \vec{\xi}_i(t), \tag{2.1}$$

where $\vec{\xi}_i(t)$ is a d-dimensional vector of uncorrelated Gaussian white noises. In order to take the best decision about the strategy, agents select the drift term $\vec{a}_i$ by minimizing (maximizing) a certain cost (gain) functional, defined, for example in this case, as

$$c_i[\vec{a}](\vec{X}, t) = \mathbb{E}\left\{ \int_t^T \left[\frac{\mu}{2} (\vec{a}_i(\tau))^2 - V_i(\vec{X}(\tau), \tau) \right] d\tau + c_{Ti}(\vec{X}(T)) \right\}, \tag{2.2}$$

where $\vec{X}(t) = (\vec{X}_1(t), \ldots, \vec{X}_N(t))$ and $\vec{a} = (\vec{a}_1, \ldots, \vec{a}_N)$. There are various terms in equation (2.2) that need to be explained. First of all, c_T represents a *terminal cost* that each player knows from the beginning. Then, $V(\vec{X}, \tau)$ is a potential that acts on each player collectively and that describes how agents interact with each other and with the environment. Finally, the presence of the square of the control parameter $\vec{a}$ means that we are dealing with *quadratic games*, which have been widely described in [34]. This is not the only possible choice.

At this point some simplifications are in order. First of all, we assume that each player is identical, meaning that $\forall i$, $V_i = V$, $c_{Ti} = c_T$ and $\sigma_i = \sigma$. Finally, the fundamental assumption that we make is that both the potential and the final cost depend on the players' positions only through the empirical density

$$\tilde{m}(\vec{x}, t) = \frac{1}{N} \sum_{i=1}^{N} \delta(\vec{x} - \vec{X}_i(t)).$$

Then, we take the limit for a large number of players $N \to +\infty$. In this case, if we define $m(\vec{x}, t) = \mathbb{E}[\tilde{m}(\vec{x}, t)]$, we can then substitute $m(\vec{x}, t)$ to $\tilde{m}(\vec{x}, t)$. This means that we are not interested anymore in the description of every single trajectory, but in overall distribution of players in the space. The cost term can be now written as

$$c[\vec{a}](\vec{x}, t) = \mathbb{E}\left\{ \int_t^T \left[\frac{\mu}{2} (\vec{a}(\tau))^2 - V[m](\vec{x}, \tau) \right] d\tau + c_T[m](\vec{x}, T) \right\}. \tag{2.3}$$

Finally, the only type of potential we will consider is of the form

$$V[m](\vec{x}, t) = g m(\vec{x}, t) + U_0(\vec{x}, t), \tag{2.4}$$

where g is a coupling term. A negative value of g makes the density term in the integral of equation (2.3) positive, and, if it must be minimized, this means that

naturally the systems will adjust to a low density, resulting in *repulsive interactions*. Conversely, $g > 0$ means *attractive interactions*. Finally, we introduce the *value function*, obtained by minimizing the cost functional

$$u(\vec{x}, t) = \inf_{\vec{a}} c[\vec{a}](\vec{x}, t). \tag{2.5}$$

At this point we are able to introduce the first of the two fundamental equations that describe the dynamics of a game. In order to do so however, we must think about the optimization of, for example, the path to reach point C from point A passing through point B. Because agents can optimize their strategy at any time, it is possible to show that optimizing the whole path gives the same result as joining together the paths obtained by optimizing separately the way from A to B and from B to C. This idea lies behind the *dynamic programming principle* [7], that allows us to write

$$u(\vec{x}, t) = \inf_{\vec{a}} \mathbb{E}\left\{ \int_t^{t+dt} \left[\frac{\mu}{2} (\vec{a}(\tau))^2 - V[m](\vec{x}, \tau) \right] d\tau \right\} + u(\vec{x} + d\vec{x}, t + dt), \tag{2.6}$$

that is called *Bellman equation*. Now we observe that

$$u(\vec{x} + d\vec{x}, t + dt) \simeq u(\vec{x}, t) + \frac{d}{dt} u(\vec{x}, t) dt,$$

and the time derivative of the value function can be computed with *Ito chain rule* [19], obtaining

$$u(\vec{x} + d\vec{x}, t + dt) \simeq u(\vec{x}, t) + \left[\vec{\nabla} u \cdot \vec{a} + \partial_t u + \frac{\sigma^2}{2} \Delta u \right] dt. \tag{2.7}$$

Then, we can take the inf over $\vec{a}$ for both sides of the equation and obtain

$$u(\vec{x} + d\vec{x}, t + dt) \simeq u(\vec{x}, t) + \partial_t u dt + \frac{\sigma^2}{2} \Delta u dt + \left(\inf_{\vec{a}} \vec{\nabla} u \cdot \vec{a} \right) dt, \tag{2.8}$$

that we can substitute inside equation (2.6), giving

$$0 = \inf_{\vec{a}} \left[\frac{\mu}{2} (\vec{a}(t))^2 + \vec{\nabla} u \cdot \vec{a}(t) \right] + \partial_t u + \frac{\sigma^2}{2} \Delta u - V[m](\vec{x}, t). \tag{2.9}$$

The optimal control can be easily evaluated by taking the d-dimensional derivative with respect to $\vec{a}$ of the expression in squared brackets and, putting it equal to zero, the solution is obtained and is equal to

$$\vec{a}^* = -\frac{\vec{\nabla} u}{\mu}, \tag{2.10}$$

which can be plugged back into equation (2.9) to obtain the *Hamilton-Jacobi-Bellman equation* (HJB).

$$\begin{cases} \partial_t u + \frac{\sigma^2}{2}\Delta u - \frac{(\vec{\nabla} u)^2}{2\mu} = V[m] \\ u(\vec{x}, t = T) = c_T(\vec{x}) \end{cases} \tag{2.11}$$

This is a backward differential equation, that is built starting from its solution at time $t = T$

Now, given that each agent's position is supposed to evolve following a Langevin equation, the density of players satisfies

$$\partial_t m = \frac{\sigma^2}{2}\Delta m - \vec{\nabla} \cdot (m\vec{a}^*),$$

that is the *Fokker-Planck* equation. By substituting the value of the optimal control obtained in (2.10) we obtain

$$\begin{cases} \partial_t m - \frac{\sigma^2}{2}\Delta m + \frac{1}{\mu}\vec{\nabla} \cdot (m\vec{\nabla} u) = 0 \\ m(\vec{x}, t = 0) = m_0(\vec{x}) \end{cases} \tag{2.12}$$

Equations (2.11) and (2.12) constitute a backward-forward system. Starting from an initial density value, HJB equation informs FPE on incoming events. In fact, after HJB chooses the best possible value function, the FPE finds the next best density. It is in this process of interaction between the two equation that lies the predictive ability of MFG. We will see this in more details in the following.

2.2 Changes of variables

Now that we have built all the tools of MFG, we are left with a set of coupled equations which is not trivial to solve. A very wise approach has been devised in [34], where a *Cole-Hopf transformation* is performed and the problem is cast in a more familiar setting for many physicists. In fact, let us considers the transformation

$$u(\vec{x}, t) = -\mu\sigma^2 \log \Phi(\vec{x}, t), \tag{2.13}$$

and substitute into equation (2.11). We then get to the equation

$$\mu\sigma^2 \partial_t \Phi = -\frac{\mu\sigma^4}{2}\Delta\Phi - V[m]\Phi, \tag{2.14}$$

a standard heat equation, with terminal condition

$$\Phi(\vec{x}, t = T) = e^{-\frac{c_T(\vec{x})}{\mu\sigma^2}}. \tag{2.15}$$

Now we can also define

$$\Gamma(\vec{x},t)=\frac{m(\vec{x},t)}{\Phi(\vec{x},t)}, \tag{2.16}$$

that, when substituting into equation (2.12), gives

$$\mu\sigma^2\partial_t\Gamma=\frac{\mu\sigma^4}{2}\Delta\Gamma+V[m]\Gamma. \tag{2.17}$$

Equations (2.14) and (2.17) only differ by a change in sign while containing all the information of the original MFG equations. The one we just performed is not the only change of variable that can be done to transform mean-field game equations into something already seen in other fields of Physics. As explained in [31], we can also perform a Madelung like change of variables defining $K(\vec{x},t)$ such that $\Phi(\vec{x},t)=\sqrt{m(\vec{x},t)}e^{K(\vec{x},t)}$ and $\Gamma(\vec{x},t)=\sqrt{m(\vec{x},t)}e^{-K(\vec{x},t)}$, that substituting in equations (2.14) and (2.17) gives

$$\begin{cases}\partial_t m+\vec{\nabla}\cdot(m\vec{v})=0,\\ \partial_t\vec{v}+\vec{\nabla}\left[\frac{\sigma^4}{2\sqrt{m}}\Delta\sqrt{m}+\frac{v^2}{2}+\frac{V[m]}{\mu}\right]=0,\end{cases} \tag{2.18}$$

where $\vec{v}$ is the velocity of agents and is defined as

$$\vec{v}=\frac{\sigma^2}{2m}\left(\Gamma\vec{\nabla}\Phi-\Phi\vec{\nabla}\Gamma\right)=-\frac{\vec{\nabla}u}{\mu}-\sigma^2\frac{\vec{\nabla}m}{2m}. \tag{2.19}$$

This is called *hydrodynamic representation*. In particular, the first equation of system (2.18) is a continuity equation. We conclude this general introduction about MFG by mentioning the important results reported by P. Cardialaguet et al. in [12]. In this work, in fact, the limit of large ending time $T\to+\infty$ is considered. Under the hypothesis that there is no explicit time dependence in the cost function (2.2), it was proved that an *ergodic solution* exists and it is valid for $0<<t<<T$. This solution is of the form $(m^e(\vec{x}),u^e(\vec{x})+\lambda_e t)$ where $m^e(\vec{x})$ and $u^e(\vec{x})$ satisfy the equations

$$\begin{cases}-\lambda_e+\frac{\sigma^2}{2}\Delta u^e-\frac{(\vec{\nabla}u^e)^2}{2\mu}=V[m^e]\\ \frac{\sigma^2}{2}\Delta m^e+\frac{1}{\mu}\vec{\nabla}\cdot(m^e\vec{\nabla}u^e)=0\end{cases} \tag{2.20}$$

In the Schrödinger representation the ergodic solutions are

$$\Phi^e=e^{-\frac{u^e}{\mu\sigma^4}},\quad \Gamma^e=\frac{m^e}{\Phi^e}, \tag{2.21}$$

and it easy to prove that they both follow the equation

$$\lambda_e\psi^e=-\frac{\mu\sigma^4}{2}\Delta\psi^e-V[m]\psi^e. \tag{2.22}$$

Most importantly, the knowledge of the ergodic solution gives access to the solution also of the time dependent problem, because it is possible to show that

$$\Phi(\vec{x},t) = \exp\left\{\frac{\lambda_e}{\mu\sigma^2}t\right\}\psi^e(\vec{x}), \quad \Gamma(\vec{x},t) = \exp\left\{-\frac{\lambda_e}{\mu\sigma^2}t\right\}\psi^e(\vec{x}) \tag{2.23}$$

solve equations (2.14) and (2.17) respectively.

2.3 Operator formalism

Equations (2.14) and (2.17) define what is called the *Schrödinger representation* of Mean-Field Games. In this setting, in analogy with what is done in Quantum Mechanics, it is possible to introduce operators that correspond to physical quantities once evaluated on a system state. Let us first introduce $\hat{\boldsymbol{X}} = (\hat{X}_1, \hat{X}_2)$, the position operator, that acts as multiplication; then, we define the momentum operator $\hat{\boldsymbol{P}} = -\mu\sigma^2\nabla$. Moreover, if we consider an arbitrary operator $\hat{O}$ function of $\hat{\boldsymbol{X}}$ and $\hat{\boldsymbol{P}}$, we define its average as

$$\langle\hat{O}\rangle(t) := \langle\Phi(t)|\hat{O}|\Gamma(t)\rangle = \int \mathrm{d}\boldsymbol{x}\,\Phi(\boldsymbol{x},t)\,\hat{O}\,\Gamma(\boldsymbol{x},t). \tag{2.24}$$

where Φ and Γ are solutions of equations (2.14) and (2.17). It is important to observe that, whenever $\hat{O}$ depends only on $\hat{\boldsymbol{X}}$ then its averages is actually the expected value with respect to the density. In fact we can write

$$\langle\hat{O}\rangle(t) = \int \mathrm{d}\boldsymbol{x}\, m_t(\boldsymbol{x})O(\boldsymbol{x}) \tag{2.25}$$

We would now like to recover a very famous result in quantum mechanics. In order to do so, we differentiate with respect to time equation (2.24) and obtain

$$\begin{aligned}\frac{\mathrm{d}}{\mathrm{d}t}\langle\hat{O}\rangle &= \int\frac{\mathrm{d}\Phi}{\mathrm{d}t}\hat{O}\Gamma + \int\Phi\frac{\mathrm{d}\hat{O}}{\mathrm{d}t}\Gamma + \int\Phi\hat{O}\frac{\mathrm{d}\Gamma}{\mathrm{d}t}\\ &= \langle\frac{\mathrm{d}\hat{O}}{\mathrm{d}t}\rangle - \frac{1}{\mu\sigma^2}\int\Phi(\hat{O}\hat{H}-\hat{H}\hat{O})\Gamma\\ &= \langle\frac{\mathrm{d}\hat{O}}{\mathrm{d}t}\rangle - \frac{1}{\mu\sigma^2}\langle[\hat{O},\hat{H}]\rangle\end{aligned}$$

The second line is obtained from equations (2.14) and (2.17) and defining the Hamiltonian operator

$$\hat{H} = -\frac{\hat{\boldsymbol{P}}}{2\mu} - V[m_t](\hat{\boldsymbol{X}}). \tag{2.26}$$

What we recovered is the analogous in this framework of the *Ehrenfest theorem*. This analogy is surprising but up to a point, considering that the equations we are dealing with are mathematically very similar to the usual Quantum Mechanics ones. Now that we have obtained this result we can even go a bit further and recover other familiar relations that will highlight even more the connection between the two fields of study. In fact, we can recover the time evolution equation of the two operators momentum and position. By using the Ehrenfest theorem one gets that

$$\begin{aligned}\frac{\mathrm{d}}{\mathrm{d}t}\langle\hat{\boldsymbol{X}}\rangle &= \frac{\langle\hat{\boldsymbol{P}}\rangle}{\mu}\\ \frac{\mathrm{d}}{\mathrm{d}t}\langle\hat{\boldsymbol{P}}\rangle &= \langle\hat{\boldsymbol{F}}[m_t]\rangle\,,\end{aligned}$$

where we have introduced the *force operator* $\hat{\boldsymbol{F}}[m_t] = -\nabla V[m_t](\hat{\boldsymbol{X}})$. In the case of local interaction the potential can be written as

$$V[m_t](\hat{\boldsymbol{X}}) = U_0(\hat{\boldsymbol{X}}) + f[m(\hat{\boldsymbol{X}})]. \tag{2.27}$$

In this case it is possible to broaden the connection with the mathematical structure of quantum mechanics by defining an action functional

$$S[\Phi,\Gamma] = \int_0^T \mathrm{d}t \int_{\mathbb{R}^2} \mathrm{d}\boldsymbol{x}\left[-\frac{\mu\sigma^2}{2}(\Phi\partial_t\Gamma - \partial_t\Phi\Gamma) - \frac{\mu\sigma^4}{4}\nabla\Phi\cdot\nabla\Gamma + \Phi U_0(\boldsymbol{x})\Gamma + F[\Phi\Gamma]\right]$$

where $F(m) = \int^m f(m')dm'$. By optimizing S, by taking the variational derivative $\delta S\backslash\delta\Phi$ and $\delta S\backslash\delta\Gamma$ one recover equations (2.14) and (2.17). At this point we can also introduce the notion of energy by defining the *total energy* and related quantities $E_{tot} := E_{kin} + E_{pot} + E_{int}$ where the three terms are defined respectively

$$\begin{aligned}E_{kin} &= \frac{1}{2\mu}\langle\hat{\boldsymbol{P}}\rangle\,,\\ E_{pot} &= \langle U_0(\boldsymbol{x})\rangle\,,\\ E_{int} &= \int \mathrm{d}\boldsymbol{x} F[m(\boldsymbol{x},t)].\end{aligned}$$

Finally, we observe that since the integrand of the functional S does not depend explicitly on time, by Noether theorem we know that there exist a conserved quantity along the trajectory of the solution of the optimization. This so called *Noether charge* is the quantity E_{tot} that we just defined.

2.4 Exact results

As we developed the foundations of Mean-Field Games, it is now time to stretch it a bit and see a couple of simple example that can be solved exactly. This, as will be also for us, is rarely the case. Most of the time when trying to apply the equations to some real life problem, exact solutions are nothing but a mirage. In this section we will only consider the non interacting case, the case of local attractive potential in absence of an external potential and the quadratic potential.

2.4.1 Non interacting case

The first exactly solvable case we will consider is for $g = 0$. This assumption means that players choose their strategy regardless of what others are doing, therefore losing the strategic side of the game. Anyway, this is just a pedagogical example that allows us to dig a bit deeper into Mean-Field Games and what they can do and in what situation they can be employed. Under these hypothesis equations (2.14) and (2.17) become

$$\mu\sigma^2\partial_t\Phi = \hat{H}_0\Phi,$$
$$\mu\sigma^2\partial_t\Gamma = -\hat{H}_0\Gamma,$$

with boundary conditions respectively

$$\Phi(\boldsymbol{x}, T) = \Phi_T(\boldsymbol{x}),$$
$$\Gamma(\boldsymbol{x}, 0) = \frac{m_0(\boldsymbol{x})}{\Phi(\boldsymbol{x}, 0)},$$

and with the Hamiltonian that has now become

$$\hat{H}_0 = -\frac{\hat{\boldsymbol{P}}^2}{2\mu} - U_0(\boldsymbol{x}). \tag{2.28}$$

Under the hypothesis that the Hamiltonian operator is Hermitian, let us consider a basis of the function space given by the eigenvectors $\{\psi_n\}_{n\in\mathbb{N}}$ of the Hamiltonian $\hat{H}_0$. Then, being this a basis, we can write both Φ and Γ as linear combination of these basis functions. Moreover, an analogous of the time evolution operator can be built, and using this the final time dependent solution becomes

$$\Phi(\boldsymbol{x}, t) = \sum_{n\in\mathbb{N}} \varphi_n e^{-\frac{\lambda_n(T-t)}{\mu\sigma^2}} \psi_n(\boldsymbol{x})$$
$$\Gamma(\boldsymbol{x}, t) = \sum_{n\in\mathbb{N}} \gamma_n e^{-\frac{\lambda_n t}{\mu\sigma^2}} \psi_n(\boldsymbol{x})$$

In this expression λ_n are the eigenvalues of $\hat{H}$ and are ordered such that $\lambda_0 \leq \lambda_1 \leq \lambda_2 ...$ and so on. The coefficients φ_n are fixed using the boundary conditions at $t = T$. In fact we have that

$$\varphi_n = \int \mathrm{d}\boldsymbol{x}\, \psi_n(\boldsymbol{x})\Phi_T(\boldsymbol{x}), \tag{2.29}$$

and an analogous reasoning can be done for γ_n coefficients. While losing the main properties of games, this example is still important and pedagogical, because it shows that far from time boundaries, c'est à dire after enough time from the beginning of the game and enough time before its end, we recover indeed the ergodic solution. In fact, let us define the *characteristic time*

$$\tau_{erg} = \frac{\mu\sigma^2}{\lambda_1 - \lambda_0}. \tag{2.30}$$

Now it easy to observe that

$$\begin{cases} \Phi(\boldsymbol{x}, t) \simeq \varphi_0 e^{-\frac{\lambda_0 (T-t)}{\mu\sigma^2}} \psi_0(\boldsymbol{x}), \quad t << T - \tau_{erg} \\ \Gamma(\boldsymbol{x}, t) \simeq \gamma_0 e^{-\frac{\lambda_0 t}{\mu\sigma^2}} \psi_0(\boldsymbol{x}), \quad t >> \tau_{erg} \end{cases}$$

When both conditions are fulfilled we then obtain a time independent density profile

$$m(\boldsymbol{x}, t) = m_{erg}(\boldsymbol{x}) \sim \varphi_0 \gamma_0 e^{-\frac{\lambda_0 T}{\mu\sigma^2}} \psi_0^2(\boldsymbol{x}), \tag{2.31}$$

to which the solution converges exponentially fast.

2.4.2 Local attractive interaction

We now focus on another quite extreme case, that of an external potential negligible with respect to the interaction between agents. We will here consider only the one dimensional case. We are thus considering a potential of the form

$$V[m](x, t) = g m(x, t)^\alpha, \tag{2.32}$$

where we take $\alpha > 0$ and $g > 0$. Focusing on just the ergodic problem we interestingly observe that we recover the famous Gross-Pitaevskii equation

$$-\frac{\mu\sigma^2}{2}\partial_{xx}^2 \psi^e - g(\psi^e)^{2\alpha - 1} = \lambda_e \psi^e. \tag{2.33}$$

Then, using a result introduced in [25], it is possible to recover the lowest state energy

$$\psi^e = \psi_M \left[\cosh\left(\frac{x - x_0}{\eta_\alpha} \right) \right]^{-\frac{1}{\alpha}},$$

where ψ_M is the maximum of the function that reads

$$\psi_M = \left(\frac{\lambda^e(\alpha+1)}{g}\right)^{\frac{1}{2\alpha}}.$$

The energy of this state can also be computed and it is equal to

$$\lambda^e = -\frac{1}{4}\left(\frac{\Gamma(\frac{2}{\alpha})}{\Gamma(\frac{1}{\alpha})^2}\right)^{\frac{2\alpha}{2-\alpha}}\left(\frac{g}{\alpha+1}\right)^{\frac{2}{2-\alpha}}\left(\frac{2\alpha}{\mu\sigma^4}\right)^{\frac{\alpha}{2-\alpha}} \tag{2.34}$$

It is important to observe that the ergodic solution for this specific setting is a stationary density localized around some point x_0 and with spatial extension η_α

$$\eta_\alpha = \frac{2}{\sqrt{\alpha}}\left(\frac{\Gamma(\frac{2}{\alpha})^2}{\Gamma(\frac{1}{\alpha})}\right)^{\frac{2\alpha}{2-\alpha}}\left(\frac{\alpha+1}{2\alpha}\frac{\mu\sigma^4}{g}\right)^{\frac{1}{2-\alpha}}. \tag{2.35}$$

In the NLSE language this is called a *soliton*. We also observe that the spatial extension is given by the competition between the *noise*, which tends to broaden the density distribution, and the *attractive interaction*, that tries to bring everything together. Moreover, it is clear that for $\alpha = 2$ this solution is ill-defined. This is related to the fact that for $\alpha > 2$ the soliton is unstable.

2.4.3 Quadratic external potential

We end this section about exactly solvable model with one very common and pedagogical example in the quantum mechanics field. We will use the formal connection between the Mean-Field Games formulation we are currently using and the NLS theory to derive the solution of a system with a quadratic external potential in dimension one. To do this we consider the total potential

$$\tilde{V}[m](x) = -\frac{k}{2}x^2 + f(m(x)) \tag{2.36}$$

As explained in [25], we can solve this problem starting from the ansatz

$$\Phi(x,t) = e^{-\frac{\gamma(t)-xP(t)}{\mu\sigma^2}}\psi^e(x-X(t))$$
$$\Gamma(x,t) = e^{+\frac{\gamma(t)-xP(t)}{\mu\sigma^2}}\psi^e(x-X(t))$$

where $\psi^e(x)$ is the solution of the ergodic equation. Observe also that with this ansatz the resulting density is $m(x,t) = \Phi(x,t)\Gamma(x,t) = \psi_e^2(x-X(t))$, independent

of $P(t)$ and $\gamma(t)$. Inserting the ansatz into equations (2.14) and (2.17) allows to obtain

$$\begin{aligned}\dot{P}(t) &= kX(t)\\ \dot{X}(t) &= \frac{P(t)}{\mu}\\ \dot{\gamma(t)} &= \frac{k}{2}X(t)^2 + \frac{P(t)^2}{2\mu} - \lambda^e\end{aligned}$$

Where the first two equations describe the motion of the center of mass $X(t)$ of the density distribution. The third equation describes the evolution of the width of the density, and, integrated, gives

$$\gamma(t) = \frac{X(t)P(t)}{2} - \lambda_e t + \gamma_0. \tag{2.37}$$

It is also possible to obtain the expression for the evolution of the center of mass of the density, provided that the initial condition is chosen with care as explained in [34]. This is in fact

$$X(t) = x_0 \frac{\sinh \omega(T-t)}{\sinh \omega T} + x_T \frac{\sinh \omega t}{\sinh \omega T},$$

where $\omega := \sqrt{k/\mu}$.

Chapter 3

MFG model of the experiment

So far we have described in details the foundation of MFG and their mathematical structure. The way we want to apply them to the experiment of Nicolas et colleagues is by considering the parameter $\vec{a}(t)$ as the velocity of pedestrians. We think this approach is reasonable because the only thing a person has to decide at each instant when walking through a crowd is their velocity. Module and direction of the velocity will indeed determine the motion. Pedestrians optimize their velocity according to the density around them and the obstacles they encounter. Moreover, since crowded environments change quickly and a pedestrian has to adapt to many small perturbations, it also seems appropriate to describe the motion of a single person in the crowd with the Langevin equation (2.1). This is why we thought MFG could apply well to this situation.

3.1 Passing to the moving frame

The problem we are trying to model is the evolution of the density of pedestrians in a confined environment, namely a square of side L, through which a cylinder is made pass from bottom to top with constant velocity $\vec{s} = (0, s)$. We argue then that the right set of equations to describe this problem is given by MFG equations in the NLS representation that we recall

$$\mu\sigma^2\partial_t\Phi = -\frac{\mu\sigma^4}{2}\Delta\Phi - V[m]\Phi,$$
$$\mu\sigma^2\partial_t\Gamma = \frac{\mu\sigma^4}{2}\Delta\Gamma + V[m]\Gamma,$$

where in this case $V[m] = gm(\vec{x}, t) + U(\vec{x}, t)$ with $U(\vec{x}, t)$ representing the moving cylinder as an external potential equal to $+\infty$ inside a 2 dimensional disk of radius R and equal to 0 outside. This external potential introduces an explicit time

dependence in the cost function (2.2), preventing the existence of an ergodic state. To correct this problem we pass from the point of view of the laboratory to the point of view of the cylinder. In order to do so we define of the following quantities

$$\tilde{u}(\vec{x}-\vec{s}t,t)=u(\vec{x},t),\quad \tilde{m}(\vec{x}-\vec{s}t,t)=m(\vec{x},t),$$
$$\tilde{\Phi}(\vec{x}-\vec{s}t,t)=\Phi(\vec{x},t),\quad \tilde{\Gamma}(\vec{x}-\vec{s}t,t)=\Gamma(\vec{x},t).$$

In this framework the potential does not depend on time anymore and it becomes $\tilde{V}[\tilde{m}]=g\tilde{m}+\tilde{U}(\vec{x})$, with

$$\tilde{U}(\vec{x})=\begin{cases}+\infty & x<R\\ 0 & \text{otherwise}\end{cases}. \tag{3.1}$$

For all other quantities the time dependence now appears also in the position variable. In this case we observe that

$$\partial_t f(\vec{x},t)=\frac{\mathrm{d}}{\mathrm{d}t}f(\vec{x},t)=\frac{\mathrm{d}}{\mathrm{d}t}\tilde{f}(\vec{x}-\vec{s}t,t)=\partial_t\tilde{f}-\vec{s}\cdot\vec{\nabla}\tilde{f}. \tag{3.2}$$

We can then substitute expression (3.2) into equations (2.14) and (2.17) and obtain the moving frame equations

$$\mu\sigma^2\partial_t\tilde{\Phi}-\mu\sigma^2\vec{s}\cdot\vec{\nabla}\tilde{\Phi}=-\frac{\mu\sigma^4}{2}\Delta\tilde{\Phi}-V[m]\tilde{\Phi}, \tag{3.3}$$
$$\mu\sigma^2\partial_t\tilde{\Gamma}-\mu\sigma^2\vec{s}\cdot\vec{\nabla}\tilde{\Gamma}=\frac{\mu\sigma^4}{2}\Delta\tilde{\Gamma}+V[m]\tilde{\Gamma}. \tag{3.4}$$

We want to find the ergodic state of the moving frame equations. Recalling now the relationship between the ergodic state solution and the time dependent one expressed in (2.23), we observe that

$$\partial_t\tilde{\Phi}=\frac{\lambda_e}{\mu\sigma^2}\tilde{\Phi}=\frac{\lambda_e}{\mu\sigma^2}e^{\frac{\lambda_e}{\mu\sigma^2}t}\tilde{\Phi}^e,\quad \partial_t\tilde{\Gamma}=-\frac{\lambda_e}{\mu\sigma^2}\tilde{\Gamma}=-\frac{\lambda_e}{\mu\sigma^2}e^{-\frac{\lambda_e}{\mu\sigma^2}t}\tilde{\Gamma}^e.$$

These expressions can finally be substituted inside equations (3.3) and (3.4) to get rid of any explicit time dependence. Simplifying all the exponentials we finally obtain

$$\frac{\mu\sigma^4}{2}\Delta\tilde{\Phi}^e-\mu\sigma^2\vec{s}\cdot\vec{\nabla}\tilde{\Phi}^e+\tilde{V}[\tilde{m}^e]\tilde{\Phi}^e=-\lambda_e\tilde{\Phi}^e, \tag{3.5}$$
$$\frac{\mu\sigma^4}{2}\Delta\tilde{\Gamma}^e+\mu\sigma^2\vec{s}\cdot\vec{\nabla}\tilde{\Gamma}^e+\tilde{V}[\tilde{m}^e]\tilde{\Gamma}^e=-\lambda_e\tilde{\Gamma}^e. \tag{3.6}$$

These equations contain no time dependent quantities anymore. The last problem to solve before starting devising a numerical scheme to solve the equations is to find the right boundary conditions in order to fix the solutions.

3.2 Choosing boundary condition

In order to solve equations (3.5) and (3.6), it is important to understand what boundary conditions to impose in order to fix a solution. In the experiment of the moving cylinder, far from it people were not moving, meaning that, far from the obstacle, the velocity of the pedestrians was null in the laboratory frame. This means that, when passing to the moving frame, agents at the boundary should move with velocity $-\vec{s}$. From the hydrodynamic representation (2.18) of MFG, one knows that the definition of velocity in terms of Φ and Γ is

$$\vec{v} = \frac{\sigma^2}{2m}\left(\Gamma\vec{\nabla}\Phi - \Phi\vec{\nabla}\Gamma\right) = -\frac{\vec{\nabla}u}{\mu} - \sigma^2\frac{\vec{\nabla}m}{2m}. \tag{3.7}$$

This definition is valid also if we consider the ergodic state of the moving frame

$$\vec{v} = \frac{\sigma^2}{2\tilde{m}^e}\left(\tilde{\Gamma}^e\vec{\nabla}\tilde{\Phi}^e - \tilde{\Phi}^e\vec{\nabla}\tilde{\Gamma}^e\right) = -\frac{\vec{\nabla}\tilde{u}^e}{\mu} - \sigma^2\frac{\vec{\nabla}\tilde{m}^e}{2\tilde{m}^e}. \tag{3.8}$$

Now, we know that at the boundary the density should be constant therefore we can drop the gradient of $\tilde{m}^e$ in the last expression; this means that we can just force the equality

$$\frac{\vec{\nabla}\tilde{u}^e}{\mu} = \vec{s}, \tag{3.9}$$

in order to have the right velocity far from the obstacle. Now, recalling that $\tilde{u}^e = -\mu\sigma^2\log\tilde{\Phi}^e$, we can substitute in equation (3.9) and obtain

$$\sigma^2\frac{\vec{\nabla}\tilde{\Phi}^e}{\tilde{\Phi}^e} = -\vec{s},$$

from which we obtain the equations

$$\frac{\partial\tilde{\Phi}^e}{\partial x} = 0, \quad \frac{\partial\tilde{\Phi}^e}{\partial y} = -\frac{s}{\sigma^2}\tilde{\Phi}^e,$$

that can be solved yielding the ergodic asymptotic solution

$$\tilde{\Phi}^e(x,y) = Ce^{-\frac{s}{\sigma^2}y}. \tag{3.10}$$

In order to fix C, we observe that far from the cylinder the density should be the average one, that we call m_0. Therefore, recalling that $\tilde{\Phi}^e\tilde{\Gamma}^e = \tilde{m}^e$, we can take $C = \sqrt{m_0}$ and thus have that $\tilde{\Gamma}^e(x,y) = \sqrt{m_0}e^{\frac{s}{\sigma^2}y}$. An interesting thing we notice is that a new parameter has emerged, one that relates the diffusion coefficient and

the velocity of the cylinder. We will call this parameter $f = \frac{s}{\sigma^2}$. This boundary solutions contain all the information necessary to find the solution to the entire equations, since the only conditions Φ and Γ have to satisfy at the boundary are those related to the velocity and the value of the average density.

Having found the expression of the asymptotic solution not only gives us the boundary conditions to solve the equations; in fact, it also allows us to fix λ_e, giving us the correct ergodic state. Since λ_e is a constant quantity it can be computed using the asymptotic solution and we are sure it will also be valid for the general solution. To fix the parameter λ_e, we can indeed substitute the asymptotic form (3.10) into (3.5), which has to be valid far from the cylinder. This leads to

$$\frac{\mu\sigma^4}{2}\frac{s^2}{\sigma^4}\tilde{\Phi}^e + \mu\sigma^2\frac{s^2}{\sigma^2}\tilde{\Phi}^e + gm_0\tilde{\Phi}^e = -\lambda_e\tilde{\Phi}^e, \tag{3.11}$$

giving

$$\lambda_e = -gm_0 - \frac{3}{2}\mu s^2 \ . \tag{3.12}$$

3.3 Numerical solution

Now that we have solved the problem of boundary conditions, our goal is to find a numerical scheme to solve the equations. Let us consider equation (3.5).

$$\frac{\mu\sigma^4}{2}\Delta\tilde{\Phi}^e - \mu\sigma^2\vec{s}\cdot\vec{\nabla}\tilde{\Phi}^e + \tilde{V}[\tilde{m}]\tilde{\Phi}^e = -\lambda_e\tilde{\Phi}^e.$$

We will use the cylindrical potential (3.1), implemented numerically as $\tilde{V}_0 V(\vec{x})$

$$V(\vec{x}) = \begin{cases} 1 & x < R \\ 0 & \text{otherwise} \end{cases} \ . \tag{3.13}$$

Then, we first consider $g = 0$, therefore the equation we have to solve numerically are

$$\frac{\mu\sigma^4}{2}\Delta\Phi - \mu\sigma^2 s\partial_y\Phi + V_0 V(\vec{x})\Phi = -\lambda\Phi, \tag{3.14}$$

where we dropped the tilde and the denotation of ergodic state, and already used the fact that the velocity of the cylinder is vertical. Now we are ready to implement the numerical scheme. We want to solve the equation on a box of side L, therefore, first of all, we define a meshgrid in Python of $N \times N$ points corresponding to the (x, y) coordinates in Euclidean space. Then we define the matrixces $\Phi \in \mathbb{R}^{N,N}$ and $\Gamma \in \mathbb{R}^{N,N}$ that we have to evaluate. We will then use the meshgrid matrix of

coordinates to plot the values of the two matrices Φ and Γ. In order to do this, we first write the discrete form of equation (3.14)

$$\frac{\mu\sigma^4}{2dx^2}(\Phi_{i-1,j}+\Phi_{i+1,j}+\Phi_{i,j-1}+\Phi_{i,j+1}-4\Phi_{i,j})-\mu\sigma^2 s\frac{\Phi_{i,j+1}-\Phi_{i,j-1}}{2dy}+V_0V_{i,j}\Phi_{i,j}=-\lambda\Phi_{i,j},$$

where we choose $dx = dy$. Then make the term $\Phi_{i,j}$ explicit and obtain

$$\Phi_{i,j}^{k+1}=\frac{\frac{\mu\sigma^4}{2}(\Phi_{i-1,j}^k+\Phi_{i+1,j}^k+\Phi_{i,j-1}^k+\Phi_{i,j+1}^k)-\frac{\mu\sigma^2}{2}sdx(\Phi_{i,j+1}^k-\Phi_{i,j-1}^k)}{2\mu\sigma^4-\lambda dx^2-V_0V_{i,j}dx^2}.$$

This is the recursive rule that updates $\Phi_{i,j}$ until convergence. Starting from an initial guess of the solution, but with boundary conditions given by solution (3.10), the algorithm updates all the points of the Φ matrix simultaneously, just shifting rows or columns to sum neighboring points. At each step, the relative distance with the matrix at the previous iteration is computed and the algorithm halts as soon as a threshold is reached. This method is called Jacobi method and in practice it takes the initial guess for the solution and it connects it smoothly to the boundary conditions while solving the equation. The same can be done for Γ, just changing sign of s. Now that we have found both Φ and Γ, we can also solve the case for $g \neq 0$. We do this by starting with an initial density matrix with all entries equal to m_0. Then, we use the Jacobi method to compute Φ and Γ but this time also including the density term. Finally, we just use that $m = \Phi\Gamma$, update the density and compute again Φ and Γ. We repeat this operation until convergence of m.

3.4 Results

Let us start by defining some key quantities. First of all, in the two dimensional setting we framed our problem in, it is possible to define the *kinetic energy* and the *interaction energy* as, respectively,

$$E_{kin}=\frac{\mu\sigma^4}{2\nu^2},\quad E_{int}=g\bar{\rho}.$$

In the definition of the kinetic energy we introduced ν, that is the *healing length*. This, as explained in [9], corresponds to the distance after which a perturbed density of pedestrian recovers its bulk value. This emerges from the balance between interaction and diffusion. Therefore, equating the two energies just defined we obtain

$$\nu=\sqrt{\frac{\mu\sigma^4}{2|g|m_0}}. \tag{3.15}$$

Then, it is also possible to define the *healing time* $\tau = |\mu\sigma^2/g\bar{\rho}|$, which is the time required for the solution to recover from a perturbation. These two quantities can then be used to obtain another important length of the problem: the *healing speed*, defined as

$$\xi = \frac{\nu}{\tau} = \sqrt{\frac{|g|m_0}{2\mu}}, \tag{3.16}$$

that quantify the speed of recovery of the density of pedestrians to its bulk value. We can use the healing speed and the healing length to describe all possible scenarios we can deal with in this setting, given that ξ and ν are both defined in terms of g and that once we fix both the size of the room and the size of the obstacle we can tune the other parameters μ and σ independently. Figure 3.1 shows the 4 main regimes we can find our solution in. Figure 3.1a shows the case $\xi > s, \nu > R$, in which the crowd adjusts easily to the passage of the obstacle, thanks to a healing speed larger than the speed of the intruder. In figure 3.1b, on the other hand, a healing length smaller than the size of the cylinder means that only those in its proximity are impacted. In this case we can see the darker shadows at the sides of the obstacle, corresponding to an increase in density: pedestrians make space for the intruder as soon as they encounter it, with little anticipation. Figures 3.1c and 3.1d show the case in which the $\xi < s$. We see in this case that people make space for the incoming intruder much earlier than in the $\xi > s$ case, effectively showing some degree of anticipation. How far in space the perceived presence of the obstacle causes the crowd to start moving is determined by the value of the healing length. These observations are confirmed and amplified when the velocity field of pedestrian is analyzed as figure 3.2 shows. In figure 3.2a we see how only people in the vicinity of the obstacle are affected by it, and they move relatively slowly to adjust to its presence. Moreover, we see people moving in an almost circular region around the cylinder. This feature is displayed even better in figure 3.2b, where the pattern of motion is again of a radial displacement, but the concerned area is clearly larger. We link this behavior to the fact that in both cases $\xi > s$, giving pedestrians the possibility to start reacting just when they start feeling the pressure from the incoming cylinder, without hurrying much. In fact, in figures 3.2c and 3.2d we see how $\xi < s$ implies the emergence of anticipation patterns. The two pictures show that people start reacting already far away from the obstacle, moving laterally to make room for its passage. Then, they escape the crowd's pressure filling the empty space behind the cylinder. Moving laterally then seems to be the least expensive move to perform in this context, and intuitively this makes sense, because, while being the shortest possible displacement to avoid the cylinder, it also puts the agent under the smallest possible pressure from surrounding people.

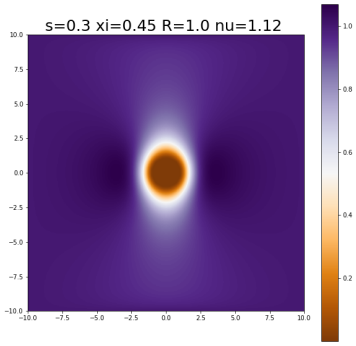

(a) $\xi > s, \nu > R$

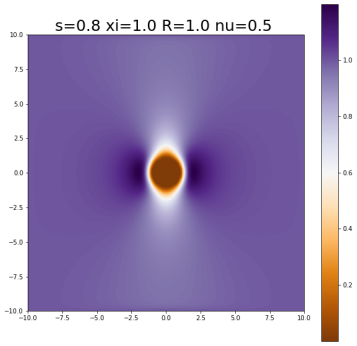

(b) $\xi > s, \nu < R$

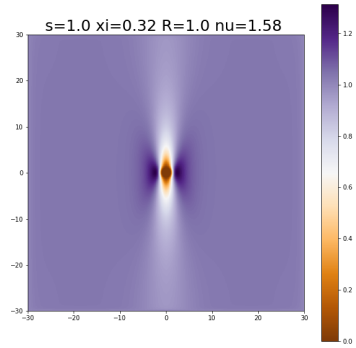

(c) $\xi < s, \nu > R$

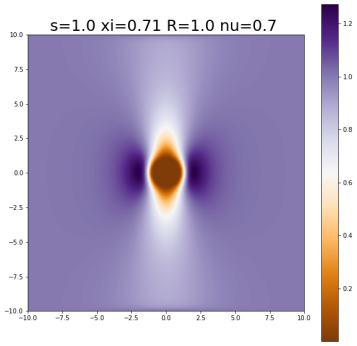

(d) $\xi < s, \nu < R$

Figure 3.1: The relations between healing length, healing speed and the velocity and size of the obstacle identify four different regimes.

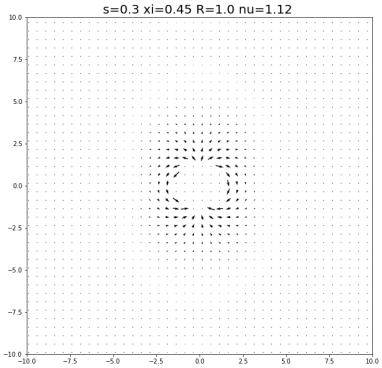

(a) $\xi > s, \nu > R$

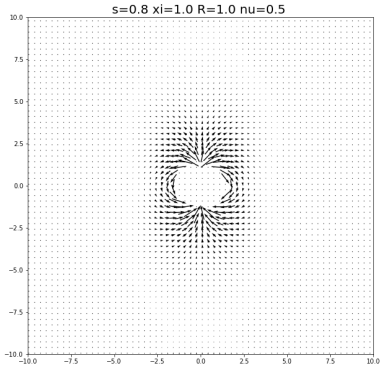

(b) $\xi > s, \nu < R$

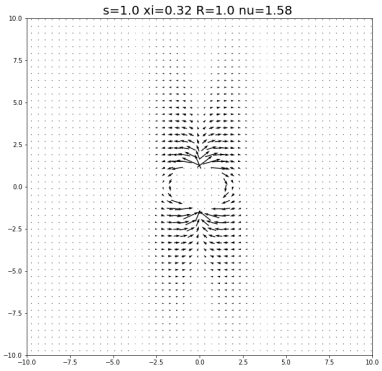

(c) $\xi < s, \nu > R$

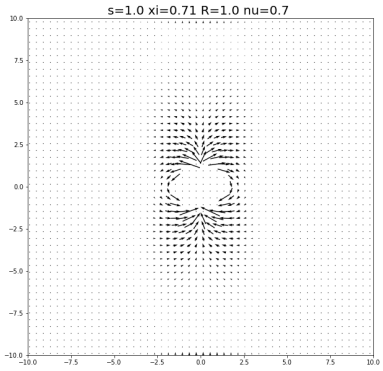

(d) $\xi < s, \nu < R$

Figure 3.2: The relations between healing length, healing speed and the velocity and size of the obstacle identify four different regimes, velocity plots.

Chapter 4

Conclusions

From what we have seen so far, we are pretty happy with our results. In fact, the passage to the moving frame not only allowed us to obtain equations easier to solve, namely equations (3.5) and (3.6), but the results it produced are qualitatively very promising. Despite the simplicity of the model, the overall behavior represented by our solution shows both of the experiment's main features, namely the ability of pedestrians to anticipate the obstacle and their reaction to the pressure from others.

4.1 Reproducing the experiment

Since we believed that our approach could be pushed even further, we also tried to get as close as possible to the quantitative behavior. We tuned the parameter σ, μ and g in order to obtain something similar to what was obtained in the experiment. In particular, we tried to match the density shown in figure 4.1a and the corresponding velocity displayed in 4.1c. We assumed that the cylinder moved at $0.75 m/s$, half the average human walking speed. The result is quite good. As we can see in figure 4.1b, additionally to the already commented qualitative agreement, we recover a value of the density of $\sim 3,5\,\mathrm{ped}/m^2$ at the sides of the obstacle, close to what is found in the experiment. Then, figure 4.1d shows the velocity field we obtained using our simulation. Plotting the velocity was not an easy task. In fact, due to the finite nature of the algorithm, some agents are considered as almost *under* the cylinder. Since these points will try to escape from it at very high velocity, plotting the simulated velocity of pedestrian in the vicinity of the intruder would result in a bunch of long arrows without any physical meaning. In order to avoid this, therefore, transparency proportional to density is introduced. In any case, the simulated velocity exhibits a behavior very similar to the experimental one. People start moving horizontally far from the obstacle in

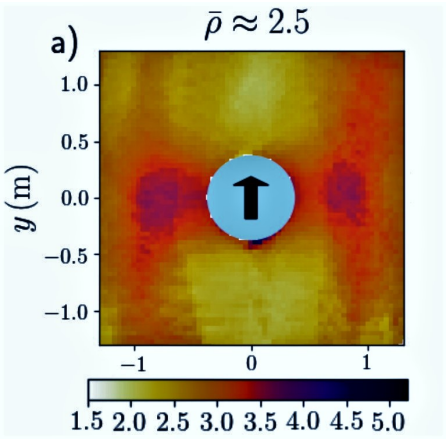

(a) Experimental density of pedestrians ($\bar{\rho} = m_0$).

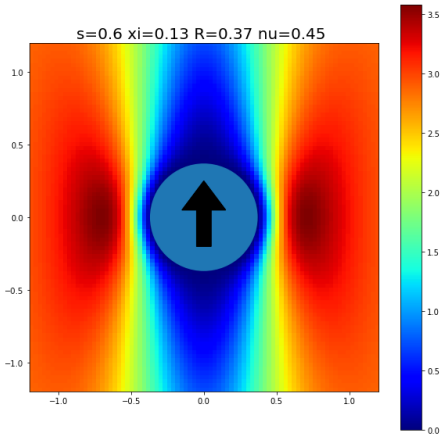

(b) Simulated density of pedestrians.

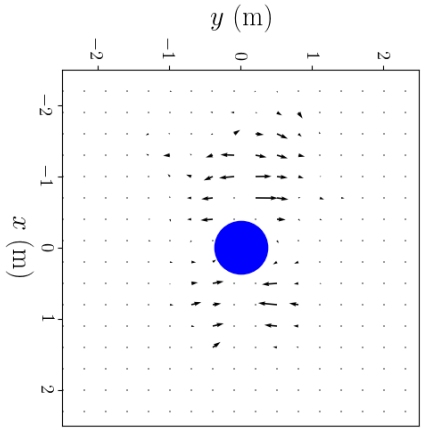

(c) Experimental velocity field.

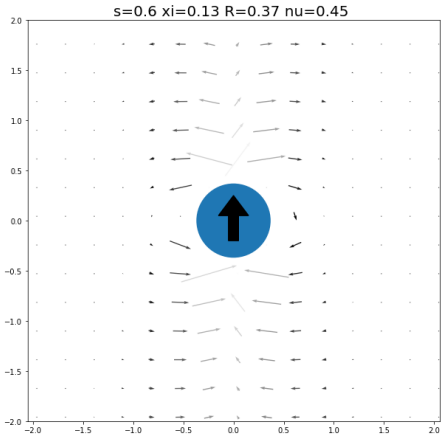

(d) Simulated velocity field.

Figure 4.1: Here are displayed both the density and the velocity field of the pedestrians. Our goal was to obtain a visually similar result to figure 1.2-b

order to avoid impacting into it. Moreover, no circular motion around the obstacle is detected, another element of similarity with respect to what is found in the experiment.

4.2 Simulating other scenarios

Now that we verified that our model gives good results in simulating the experimental data we have, we realize that something more can be done. In fact, more than just for the sake of pure knowledge, the reason behind our work is also to improve the way pedestrian dynamics is simulated, in order to be able to create safer environments and more carefully planned endeavors. Therefore we would like to see how our machinery works in simulating other environments, with, for example, more obstacles or series of them. In fact, nowadays many softwares for pedestrian dynamics are equipped with very good graphics, also to display a realistic motion of people moving in the modeled environment. However, the way they direct the motion itself relies on the velocity field obtain by the algorithm used to make predictions. Therefore, since we are able to obtain a velocity field with our algorithm, nothing prevents us, in the future, from integrating an appealing graphical simulation that has, under the hood, the simulation we provide. In this section I will present the simulation of a crowd passing through three corridors, or gates, of width $1m$ and length $2m$. Pedestrians are assumed to move uniformly towards the negative y axis with average velocity s. These are restrictive assumptions, allowing for little randomness or noise, but still important information can be extracted. The results are again very interesting. As figure 4.2a shows, what the algorithm gives is an increase in density in every corridor, with a depletion before and after every rectangle. Therefore, the model predicts the intuitive idea that people will start choosing a corridor before getting too close. They will avoid as long as possible to push into a crowded area, and then they will start moving when, because of their velocity, they will realize that not moving will lead to impact. Again, as already done in the cylinder case, we can look at the velocity field to have confirmation of our analysis. In fact, figure 4.2b shows something very close to what the density already suggested. Remark: in the figure opacity proportional to the density is introduced, so that arrows located in a very low density area are almost invisible. In this way, the black thick arrows we see in the corridors show the increase of density as well as the increase in speed. Moreover, it is interesting to observe that arrows above the rectangles start to change direction in order to avoid contact. Then, after the obstacle is passed, crowd pressure is released and the arrows pointing inward mean that pedestrians will regain space as soon as they can.

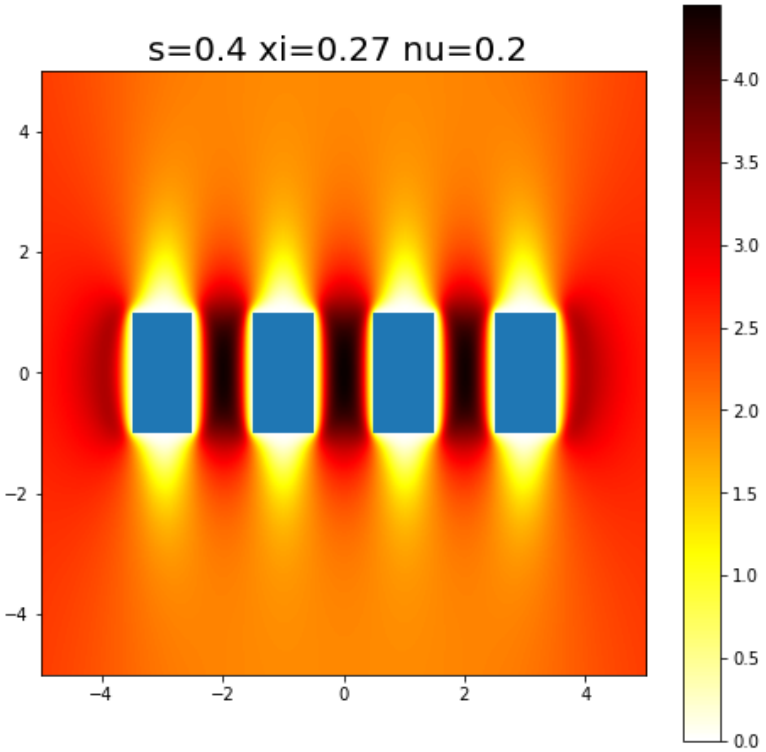

(a) Simulated density of crowd passing through three corridors

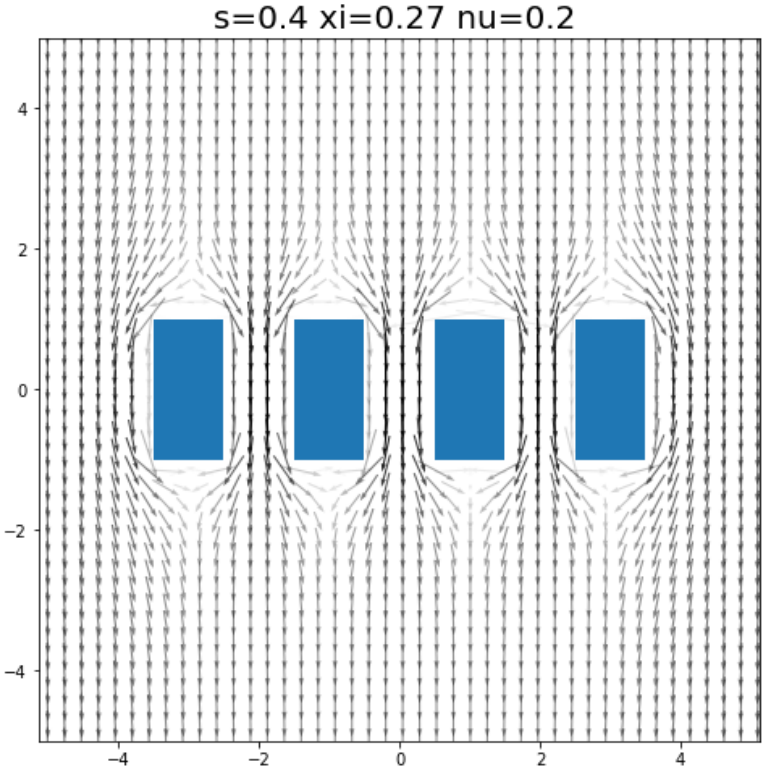

(b) Simulated velocity of crowd passing through three gates

4.3 Final remarks and future improvements

I am personally rather satisfied with these results, especially since what we used is the simplest MFG model. This, however, is just the beginning of it. We are already working on substantial improvements. First of all, we asked ourselves how a *discount factor* can be introduced, in order to force agents to optimize their strategy not for the entire game but just considering what will happen in a finite future time span. Then, it is obvious that what we obtained here is a deterministic solution, coming from deterministic equations. However, the complexity of human behavior can hardly be described as deterministic. For this reason, our next goal will be to add some *randomness* to the equations. For example, we want to consider the case in which the velocity of the cylinder is not a constant but is a random variable. Finally, we would like to introduce *congestion effects*, that, as reported in [26], already helped describing interesting phenomena like the spontaneous appearance of preferential patterns of motion. The concept of congestion simply amounts to the fact that pedestrians collectively slow down in high density areas. We think that all these improvements of the model will help us reaching a deeper understanding of Mean-Field Games in general, and we hope will give us simulations closer to reality and with interesting emerging behaviors. We will see, however, what the future holds.

Bibliography

[1] Nicolas A., Kuperman M., Ibañez S., Bouzat S., and Appert-Rolland C. Mechanical response of dense pedestrian crowds to the crossing of intruders. *Scientific Reports*, 9(105), 2019.

[2] Y. Achdou, F. J. Buera, J.-M. Lasry, Lions P.-L., and B. Moll. Partial differential equation models in macroeconomics. *Phil. Trans. R. Soc.*, 372, 2014.

[3] Y. Achdou, F. Camilli, and I. Capuzzo-Dolcetta. Mean field games: numerical methods for the planning problem.". *SIAM J. Control Optim.*, 50(1):77–109, 2012.

[4] Y. Achdou, P-N. Giraud, J.-M. Lasry, and P.-L. Lions. A long-term mathematical model for mining industries. *Appl. Math. Optim.*, 74:579–618, 2016.

[5] Yves Achdou, Martino Bardi, and Marco Cirant. Mean field games models of segregation. *Mathematical Models and Methods in Applied Sciences*, 27(01):75–113, 2017.

[6] Noha Almulla, Rita Ferreira, and Diogo Gomes. Two numerical approaches to stationary mean-field games. *Dynamic Games and Applications*, 7(4):657–682, 2017.

[7] R. Bellman, R.E. Bellman, and Rand Corporation. *Dynamic Programming*. Princeton University Press, 1957.

[8] A. Bensoussan, J. Frehse, and S. C. P. Yam. The master equation in mean field theory. *J. Math. Pures Appl.*, 103(6):1441–1474, 2015.

[9] Thibault Bonnemain, Thierry Gobron, and Denis Ullmo. Lax connection and conserved quantities of quadratic mean field games, 2020.

[10] P. Cardaliaguet. Notes on mean field games (from p.-l. lions' lectures at collège de france).

[11] P. Cardaliaguet and Lehalle C.-A. Mean field game of controls and an application to trade crowding, 2017.

[12] P. Cardaliaguet, J.-M. Lasry, P.-L. Lions, and A. Porretta. Long time average of mean field games with a nonlocal coupling. *SIAM J. Control Optim*, 51(5):3558–3591, 2013.

[13] Pierre Cardaliaguet, François Delarue, Jean-Michel Lasry, and Pierre-Louis Lions. *The Master Equation and the Convergence Problem in Mean Field Games*. Princeton University Press, 2019.

[14] R. Carmona and F. Delarue. Probabilistic analysis of mean-field games. *SIAM J. Control Optim.*, 51(4):2705–2734, 2013.

[15] René Carmona, François Delarue, and Aimé Lachapelle. Control of mckean–vlasov dynamics versus mean field games. *Mathematics and Financial Economics*, 7(2):131–166, 2013.

[16] Helbing D. *Physics of Dry Granular Media*. Springer, 1998.

[17] Helbing D. and Molnar P. Social force model for pedestrian dynamics. *Physical Review E*, 51(4282), 1995.

[18] Zanlungo F., Ikeda T., and Kanda T. Social force model with explicit collision prediction. *EPL (Europhysics Letters)*, 93(6), 2011.

[19] C.W. Gardiner. *Handbook of stochastic methods for physics, chemistry, and the natural sciences*. Springer-Verlag, 1985.

[20] D. A. Gomes and J. Saúde. Mean field games models – a brief survey. *J. Dyn. Games Appl.*, 4(2):110–154, 2014.

[21] O. Guéant. Mean field games equations with quadratic hamiltonian: a specific approach. *Math. Models Methods Appl. Sci.*, 22, 2012.

[22] M. Huang, R. P. Malhamé, and P. E. Caines. Large population stochastic dynamic games: closed-loop mckean–vlasov systems and the nash certainty equivalence principle. *Commun. Inf. Syst.*, 6(3):221–252, 2006.

[23] Arman C. Kizilkale and Roland P. Malhamé. Load shaping via grid wide coordination of heating-cooling electric loads: A mean field games based approach.

[24] Arman C Kizilkale, Rabih Salhab, and Roland P Malhamé. An integral control formulation of mean field game based large scale coordination of loads in smart grids. *Automatica*, 100:312–322, 2019.

[25] Pitaevskii L. and Stringari S. *Bose-Einstein Condensation*. Clarendon Press, Oxford, 2003.

[26] A. Lachapelle and M.-T. Wolfram. On a mean field game approach modeling congestion and aversion in pedestrian crowds. *Transportation Research Part B*, 45(10):1572–1589, 2011.

[27] J.-M. Lasry and P.-L. Lions. Jeux à champ moyen. i – le cas stationnaire. *C. R. Acad. Sci. Paris*, 343(9):619–625, 2006.

[28] J.-M. Lasry and P.-L. Lions. Jeux à champ moyen. ii – horizon fini et contrôle optimal. *C. R. Acad. Sci. Paris*, 343(10):679–684, 2006.

[29] J.-M. Lasry and P.-L. Lions. Mean field games. *Japanese Journal of Mathematics*, 2(1):229–260, 2007.

[30] Bain N. and Bartolo D. Dynamic response and hydrodynamics of polarized crowds. *Science*, 363(6422):46–49, 2019.

[31] C. J. Pethick and H. Smith. *Bose-Einstein Condensation in Dilute Gases*. Cambridge University Press, 2008.

[32] Faure S. and Maury B. Crowd motion from the granular standpoint. *Mathematical Models and Methods in Applied Sciences*, 25(03):463–493, 2015.

[33] Hoogendoorn S.P. and Bovy P.H.L. Continuum modeling of multiclass traffic flow. *Transportation Research Part B*, 34(2000):123–146, 1999.

[34] Denis Ullmo, Igor Swiecicki, and Thierry Gobron. Quadratic mean field games. *Physics Reports*, 799:1–35, 2019.